J Fluoresc (2014) 24:1841–1848
DOI 10.1007/s10895-014-1472-2

ORIGINAL PAPER

Preparation, Characterization and Solid-State Emission of Metal Complex-Cloisite Nanohybrids (MC-C, M=Ru (II) and Cu (II))

Shadpour Mallakpour · Mohammad Dinari · Hassan Hadadzadeh · Marzieh Daryanavard · Fereshteh Roudi

Received: 3 September 2014 / Accepted: 29 September 2014 / Published online: 9 October 2014

Abstract The presence of Na^+ in the Cloisite Na^+ mineral allows modification of its interlayer space to achieve a better compatibility with the host matrix and ion-exchange with a cationic metal complex. The aim of this research is to prepare two new metal complex-Cloisite (MC-C) nanohybrids using reaction of Cloisite Na^+ with the cationic Ru (II) and Cu (II) complexes, $[Ru(tpy)_2]^{2+}$ and $[Cu(Pir)(phen)(H_2O)_2]^+$, in an aqueous solution for the first time. The X-ray diffraction (XRD) analysis of the modified clays has shown an increase in its interlayer distance as compared to the unmodified Cloisite Na^+. The positions of the basal reflections in the XRD patterns of the modified clays were shifted to a higher *d* value indicating the expansion in their interlayer distances. The field-emission scanning electron microscopy has shown a homogeneous morphology for the modified clays. The thermal behavior of these novel hybrid materials was also investigated by thermogravimetric analysis. The solid state fluorescence spectra of the modified clays have shown that both cationic complexes exhibit a significant fluorescence emission at room temperature when intercalated into Cloisite.

Keywords Cloisite Na^+ · Transition metal complexes · Metal complex-cloisite · X-ray diffraction · Solid state fluorescence

S. Mallakpour (✉) · M. Dinari
Organic Polymer Chemistry Research Laboratory, Department of Chemistry, Isfahan University of Technology, Isfahan 84156-83111, Islamic Republic of Iran
e-mail: mallak@cc.iut.ac.ir

S. Mallakpour
e-mail: mallak777@yahoo.com

S. Mallakpour
e-mail: mallakpour84@alumni.ufl.edu

S. Mallakpour · M. Dinari
Nanotechnology and Advanced Materials Institute, Isfahan University of Technology, Isfahan 84156-83111, Islamic Republic of Iran

S. Mallakpour
Center of Excellence in Sensors and Green Chemistry, Department of Chemistry, Isfahan University of Technology, Isfahan 84156-83111, Islamic Republic of Iran

H. Hadadzadeh · M. Daryanavard
Department of Chemistry, Isfahan University of Technology, Isfahan 84156-83111, Islamic Republic of Iran

F. Roudi
Department of Chemistry, Hakim Sabzevari University, Sabzevar 9617976487, Islamic Republic of Iran

Introduction

Design and construction of transition metals complexes adsorbed onto solid surfaces are currently of interest in the field of catalysis, solid-state luminescence, porosity, sensors, magnetism, optoelectronic, molecular recognition, supramolecular chemistry, and antibacterial activity [1–13]. A successful approach to preparation of these materials is to select suitable cationic metal complexes and solid surfaces.

Clay minerals are very versatile materials with a wide range of applications such as paper coating, foundry molds, ceramics and building materials, pharmaceuticals, absorbents, ion-exchangers, catalysts, and catalytic supports [14]. These applications are controlled by the physicochemical properties of clays and some of these properties can be improved through the experimental modifications of raw materials [14–17]. The development of methods for preparation of modified clays has received a considerable attention in the last decades [18, 19]. Among the many types of layered silicates, sodium montmorillonite (MMT) is the most commonly used owing to its natural abundance and high aspect ratio. MMT is a naturally occurring 2:1 phyllosilicate with approximate diameter of

100 nm and thickness of 1 nm. Its crystal lattice consists of two-dimensional layers in which a central octahedral sheet of alumina or magnesia is fused to two external silica tetrahedrons by the tip so that the O^{2-} ions of the octahedral sheet also belong to the tetrahedral sheets. The isomorphic substitution of Al^{3+} by Mg^{2+} or Fe^{2+}, and Si^{4+} by Al^{3+} or Fe^{3+}, leads to formation of a negative layer in clay. The cationic-exchange capacity (CEC) is about 80–120 meq/100 g, which indicates the necessary amount of cations to balance the negative charge [20–26]. Cloisite Na^+ is a synthetic layered silicate and has high ion-exchange capacity [27]. The presence of Na^+ allows modification of its interlayer space and ion-exchange with different cations such as a cationic metal complex.

Efficient solid-state luminescent materials are very important in science and technology. Nevertheless, to the best of our knowledge, the photophysical and photochemical properties of fluorophore metal complexes intercalated into the solid powdered Cloisite have not been investigated. In our previous study, we reported the insertion of fluorophore dyes between the Cloisite interlayer distances for preparation of novel organoclays [28]. Therefore, we report here the preparation of two novel fluorescent metal complexes-Cloisite (MCs-C) nanohybrids through a cationic-exchange of Cloisite Na^+ by the cationic Ru (II) and Cu (II) complexes, $[Ru(tpy)_2]^{2+}$ and $[Cu(Pir)(phen)(H_2O)_2]^+$ (where tpy=2,2′:6′,2″-terpyridine, Pir=4-hydroxy-2-methyl-*N*-2-pyridyl-2H-1,2-benzothiazine-3-carboxamide-1,1-dioxide, and phen=1,10-phenanthroline), in an aqueous solution. Two MCs-C nanohybrids were characterized by X-ray diffraction (XRD), Fourier transform infrared spectroscopy (FT-IR), solid-state fluorescence spectroscopy, and thermal gravimetric analysis (TGA) techniques. The morphology of the MCs-C samples was determined by field-emission scanning electron microscopy (FE-SEM).

Experimental

Materials

Sodium containing natural clay with the trade name Cloisite Na^+ was obtained from the Southern Clay Products Inc., Texas, USA. Cloisite Na^+ has a cation-exchange capacity (CEC) of 92.6 meq/100 g. Deionized water was used to prepare the solutions of the Ru (II) and Cu (II) complexes.

Characterization Techniques

A Perkin-Elmer spectrofluorimeter (model LS-5) was used to study of the solid state fluorescence properties of the pure complexes and MCs-C samples. FT-IR spectra were recorded with a Jasco-680 (Japan) spectrometer as KBr pellets. The interlayer spacing of the Cloisite Na^+ and MCs-C were determined with XRD. The XRD analyses were performed using the X-ray diffractometer (Bruker, D8 Advance) with Cu*Ka* radiation (λ=0.154 nm at 45 kV, 100 mA, and with a step size of 0.02° in the range of 2θ=1.2–10°). Basal spacing were determined from the position of the *d* (001) reflection. The *d*-spacing of the MCs-C was analyzed using Bragg's equation. TGA was performed with an STA503 TA at a heating rate of 10 °C/min from ambient temperature to 800 °C under nitrogen atmosphere. The morphology of MCs-C was determined using FE-SEM (HITACHI; S-4160). The powder sample was dispersed in H_2O, and then the sediment was dried at room temperature before gold coating.

Table 1 Crystal data and structure refinement for $[Ru(tpy)_2](PF_6)_2 \cdot DMF$

Chemical formula	$C_{33}H_{29}F_{12}N_7OP_2Ru$
Formula weight	930.64
Temperature (K)	293 (2)
Crystal system	Monoclinic
Space group	$P2_1/c$
a (Å)	8.7625 (5)
b (Å)	9.0034 (5)
c (Å)	44.374 (3)
β (°)	94.247 (2)
V (Å^3)	3491.2 (3)
Z	4
Calculated density (Mg/m^3)	1.771
Crystal size (mm)	0.30×0.20×0.05
F (000)	1,864
θ range (°)	2.65 to 31.68
Reflections collected	22,761
Independent reflections (R_{int})	10,609 [$R_{(int)}$=0.0406]
Data / restraints / parameters	10609 / 0 / 507
Goodness-of-fit on F^2	1.348
Final *R* indices	R_1=0.1355, wR_2=0.2785
R indices (all data)	R_1=0.1410, wR_2=0.2807
Range of *h, k, l*	−12/12, −6/12, −40/64

Single Crystal X-Ray Crystallographic Procedure

Crystallographic data and details of data collection and structure refinement of $[Ru(tpy)_2](PF_6)_2 \cdot DMF$ are listed in Table 1. A red single crystal with dimensions of 0.30×0.20×0.05 mm^3 was attached to the tip of a glass fiber and transferred to a Bruker-AXS APEXII four-circle diffractometer equipped with a CCD camera. Data were collected using graphite Mo *Kα* radiation (λ=0.71073 Å) at 293(2) K. An absorption correction was applied with the semi-empirical multiscan approach (SADABS). Structure solution and refinement were carried out using *SHELXS97* and *SHELXL97*, respectively. The structure was solved by direct methods and refined by full-matrix least-squares methods on F^2. Hydrogen

atoms were positioned geometrically and were refined as riding, with U_{iso} (H)=1.2 U_{eq} (C). All non-hydrogen atoms were refined anisotropically.

Synthesis of [Ru (tpy) $_2$] $(PF_6)_2 \cdot$DMF

$RuCl_3 \cdot xH_2O$ (0.130 g, 0.5 mmol) and $TlPF_6$ (0.524 g, 1.5 mmol) were added to a solution of tpy (0.233 g, 1.0 mmol) in 10 mL of DMF, and the dark red mixture was refluxed under a N_2 atm for 3 h. The mixture was cooled to −5 °C overnight and then filtered through Celite to remove the fine white TlCl precipitate. After removing the solvent with a rotary evaporator, the crude product of the [Ru (tpy) $_2$] $(PF_6)_2$ complex was obtained. Purification was carried out by chromatography (Al_2O_3, grade III, WA, 30×1 cm column). Elution with acetonitrile/toluene (1:1 *v*/*v*) gave a dark red band of the pure complex, which was collected, evaporated to dryness, and then recrystallized by slow diffusion of diethyl ether into a DMF solution of the [Ru (tpy) $_2$] $(PF_6)_2$ complex. After 1 week at room temperature, single crystals of [Ru $(tpy)_2$] $(PF_6)_2 \cdot$ DMF suitable for X-ray crystallography were formed in a yield of 73 % (0.340 g), which were washed with diethyl ether and vacuum dried (Scheme 1). *Anal. Calc.* for $C_{33}H_{29}F_{12}N_7OP_2Ru$ (930.34 g/mol): C, 42.60; H, 3.13; N, 10.53. Found: C, 42.31; H, 3.05; N, 10.34 %.

Synthesis of [Cu (Pir) (phen) $(H_2O)_2$] NO_3

A solution of phen (27.0 mg, 0.15 mmol) in 10 mL ethanol was added dropwise to a solution of Cu $(NO_3)_2 \cdot 3H_2O$ (36.2 mg, 0.15 mmol) in 20 mL of water and stirred for 5 h at room temperature. Piroxicam (49.7 mg, 0.15 mmol) and NaOH (6.0 mg, 0.15 mmol) were dissolved in 15 mL of ethanol and heated at 60 °C for 30 min. The Pir^- ligand solution was then added dropwise to the above solution and stirred for 10 h at room temperature. After removing the solvent with a rotary evaporator, the crude product of the [Cu (Pir) (phen) $(H_2O)_2$] NO_3 complex was obtained. The blue powder was recrystallized by slow evaporation of a water solution. After 6 days at room temperature, blue crystals of [Cu (Pir) (phen) $(H_2O)_2$] NO_3 had formed in a yield of 79 %. Anal. Calc. for $C_{27}H_{24}CuN_6O_9S$ (MW=672.13): C, 48.25; H, 3.60; N, 12.50 %; Found: C, 48.37; H, 3.62; N, 12.61 %.

Preparation of Metal Complexes-Cloisite (MCs-C)

The MCs-C nanohybrids were prepared according to an ion-exchange procedure which is a displacement of the sodium cations of Cloisite with $[Ru(tpy)_2]^{2+}$ or [Cu (Pir) (phen) $(H_2O)_2]^+$ in an aqueous solution. The equation for calculating the intercalating cationic metal complex used for a cationic-exchange reaction is expressed as follows [29]:

$$\frac{92.6}{100} \times Y \times 1.5 = \left(\frac{X}{Mw}\right) \times 1 \times 1000$$

Where 92.6/100 represents the CEC value per 100 g of Cloisite Na^+ nanoclay; 1.5 (>1) indicates the excess amount of intercalating agent used; Y is the amount of nanoclay; and X and Mw are the amount and molecular weight of the intercalating complex. In this method, for example, an aqueous solution of [Cu (Pir) (phen) $(H_2O)_2$] NO_3 was prepared by dissolving it (1.5 times of the CEC of clay) in 50 mL of deionized water at 80 °C. Separately, 1.0 g of Cloisite Na^+ was stirred with 100 mL of deionized water at 80 °C for 3 h to swell the layered-silicates. Then, the dispersed clay was added to the solution of [Cu (Pir) (phen) $(H_2O)_2$] NO_3 and the mixture was stirred at 60 °C for 6 h. The solution containing MC-C was filtered through a Whatman® filter paper and washed with the hot deionized water. The final novel MC-C hybrid was dried in the oven at 80 °C for 24 h and grounded into a fine powder using mortar and pestle with enough pressure, and then it was passed through a 325 mesh sieve.

Results and Discussion

Synthesis and Characterization of the Ru (II) and Cu (II) Complexes

The mononuclear Ru (II) and Cu (II) complexes, [Ru $(tpy)_2$] $(PF_6)_2 \cdot$DMF and [Cu (Pir) (phen) $(H_2O)_2$] NO_3, were readily prepared in good yield and the elemental analysis of the complexes are consistent with their formulations. The complexes are stable in the solid state as well as in solution. Single crystals suitable for X-ray diffraction analysis were obtained

Scheme 1 Synthesis route to [Ru $(tpy)_2$] $(PF_6)_2$ complex

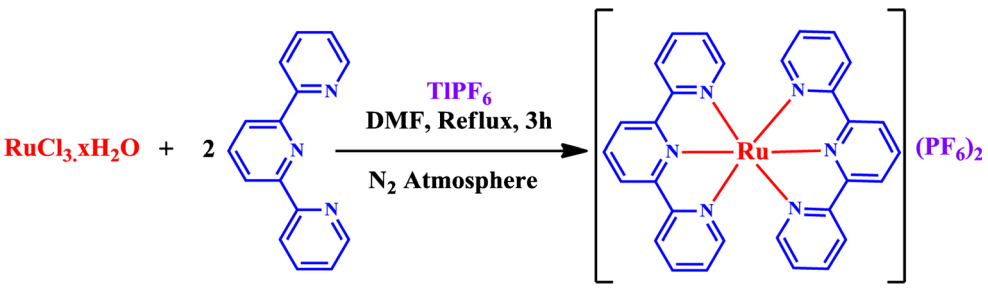

for [Ru (tpy)$_2$] (PF_6)$_2$·DMF by slow diffusion of diethyl ether into a DMF solution. An ORTEP view of the complex is shown in Fig. 1 and the selected bond lengths and angles are listed in Table 2. As shown in Fig. 1, the Ru (II) ion is hexacoordinated by six nitrogen donors of the two tpy ligands and displays a distorted octahedral geometry.

The optimized structure of [Cu (Pir) (phen) (H_2O)$_2$] NO_3 is shown in Fig. 2. Piroxicam has several possible rotamers with EZE and ZZZ conformations being the most stable ones. Piroxicam can be used as a neutral, singly deprotonated, or doubly deprotonated ligand in its transition metal complexes. It reacts as a singly deprotonated bidentate chelating ligand with ZZZ conformation towards VO^{2+}, Mn (II), Fe (III), Cu (II), MoO_2^{2+}, and UO_2^{2+} via the pyridyl nitrogen and the amide oxygen atoms. The FT-IR spectrum is shown characteristic bands associated with the coordinated Pir, Phen, and H_2O ligands to Cu (II).

Fluorescent Properties of MCs-C

The solid-state fluorescence spectra of the pure [Ru (tpy)$_2$] (PF_6)$_2$ complex and MCs-C (M = Ru (II) and Cu (II)) are illustrated in Figs. 3 and 4. For the pure [Cu (Pir) (phen) (H_2O)$_2$] NO_3 complex, no emission was observed in the solid-state due to the paramagnetic characteristic of the complex (Cu (II), d^9) which leads to the quenching of the emission through other forms of relaxations. As can be seen from Figs. 3 and 4, both cationic complexes exhibit a significant fluorescence emission at room temperature when intercalated into Cloisite. In MCs-C, the emission may come from a ligand-centered $\pi \rightarrow \pi^*$ state. Polypyridyl ligands such as tpy and phen indicate this kind of emission. In comparison to the pure Ru (II) complex (Fig. 4), its MC-C hybrid indicates an intense emission at room temperature. According to the positive charges of complexes, there is an electrostatic attraction between these cationic complexes and negative charge on the Cloisite particles. In addition, some intermolecular noncovalent interactions exist between the ligands and the counter ions of the complexes, and Cloisite. These specific interactions of the cationic complexes with Cloisite have several unique advantages in their emission such as restriction of molecular and internal-torsional motions, reduction of self-aggregation, increase of rigidity, reduction of strong excitation coupling, protection the fluorophore complex from the quenching action of dioxygen, and decrease of vibration relaxation pathways.

FT-IR Studies

The FT-IR spectra of the Cloisite Na^+, [Ru (tpy)$_2$]$^{2+}$, and its MC-C are illustrated in Fig. 5. In the FT-IR spectrum of Cloisite Na^+, the absorption bands about 3,100–3,700 cm^{-1} are due to O-H stretching and stretching band of hydrogen-bonded water. A weak broad peak at 1,630 cm^{-1} is related to H–O–H bending. The characteristic peaks at 1,115 cm^{-1} and 1,040 cm^{-1} are due to the out-of-plane Si–O stretching and in-

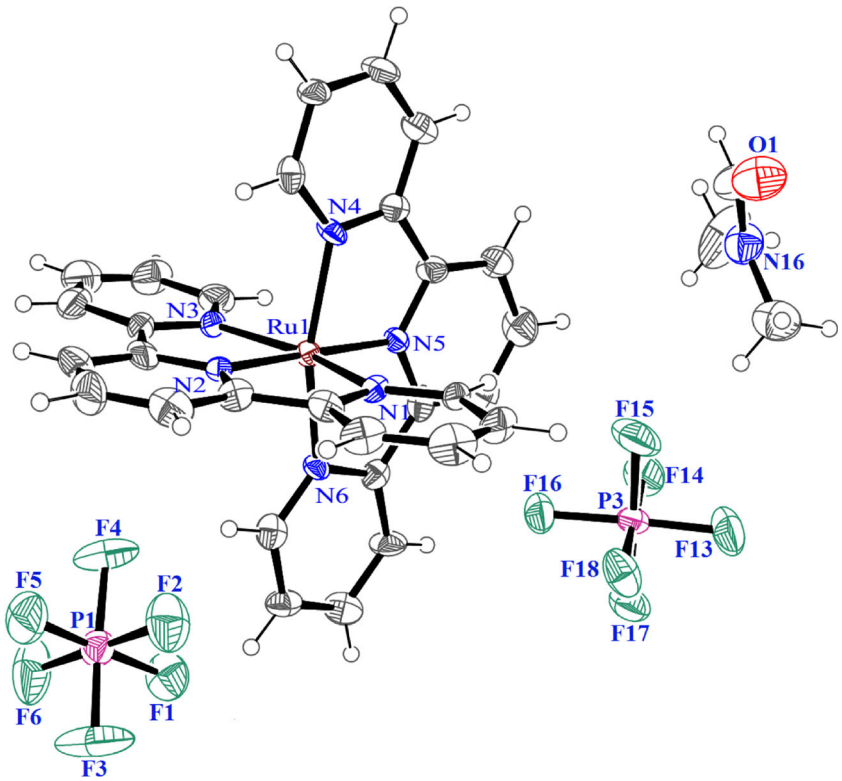

Fig. 1 ORTEP plot of [Ru (tpy)$_2$] (PF_6)$_2$DMF

Table 2 Selected bond lengths (Å) and angles (°) for Ru $(tpy)_2$] $(PF_6)_2$· DMF

Bond lengths (Å)	
Ru (1)–N (1)	2.082 (6)
Ru (1)–N (2)	1.949 (7)
Ru (1)–N (3)	2.047 (7)
Ru (1)–N (4)	2.052 (7)
Ru (1)–N (5)	1.954 (6)
Ru (1)–N (6)	2.063 (7)
Bond angles (°)	
N (2)–Ru (1)–N (5)	177.9 (3)
N (2)–Ru (1)–N (3)	81.2 (3)
N (5)–Ru (1)–N (3)	100.9 (3)
N (2)–Ru (1)–N (4)	99.5 (3)
N (5)–Ru (1)–N (4)	80.6 (3)
N (3)–Ru (1)–N (4)	89.4 (3)
N (2)–Ru (1)–N (6)	101.6 (3) .
N (5)–Ru (1)–N (6)	78.4 (3)
N (3)–Ru (1)–N (6)	92.7 (3)
N (4)–Ru (1)–N (6)	158.9 (3)
N (2)–Ru (1)–N (1)	77.5 (3)
N (5)–Ru (1)–N (1)	100.4 (3)
N (3)–Ru (1)–N (1)	158.7 (3)
N (4)–Ru (1)–N (1)	92.9 (3)
N (6)–Ru (1)–N (1)	92.7 (3)

plane Si–O stretching, respectively, for layered-silicates. Other characteristic vibration peaks at 525 and 470 cm^{-1} are for bending vibrations of Al–O and Mg–O, respectively.

In the FT-IR spectrum of $[Ru (tpy)_2] (PF_6)_2$, the characteristic bands for C = C and C = N are observed (Fig. 5a). When the $[Ru (tpy)_2]^{2+}$was intercalated into Cloisite, the FT-IR spectrum of the hybrid material shows the bands of Cloisite as well as $[Ru (tpy)_2]^{2+}$. This observation confirms the formation of the MC-C (M = Ru) hybrid.

XRD Analysis

Because of its easiness and its availability, XRD is most commonly used to probe the nanomaterials structure. By monitoring the position and intensity of the basal reflections from the distributed silicate layers, the nanohybrid structure may be predictable. The XRD patterns of Cloisite Na^+ and MCs-C (M = Ru (II) and Cu (II)) are presented in Fig. 6. The basal spacing of Cloisite Na^+ clay layers values is calculated using Bragg's Law: $n\lambda = 2dsin\theta$, where n is an integer, λ is the wavelength, θ is the glancing angle of incidence, and d is the interplanar spacing of crystal. The d-spacing of pristine Cloisite Na^+ is 1.17 nm, as calculated from the peak position $2\theta = 7.56°$. Pristine Cloisite Na^+ has a XRD peak at $2\theta = 7.56°$ due to the diffraction of the (001) crystal surface of layered-silicates with a d-spacing of 1.17 nm. An increase in the interlayer distance of Cloisite leads to a shift of the diffraction peak toward lower angles, confirming that the intercalation and surface modification of Cloisite Na^+ have been occurred. After the cation-exchange reaction with the cationic Ru (II) or Cu (II) complex, the peaks of the MCs-C are shifted to a new position at $2\theta = 2.63°$ (d=3.35 nm) and $2\theta = 3.10°$ (d= 2.855 nm), respectively. This means that the basic structures of Cloisite Na^+ are kept, the layers are only propped open, and the basal distances are increased significantly, providing evidence that the intercalation with the metal complexes has occurred.

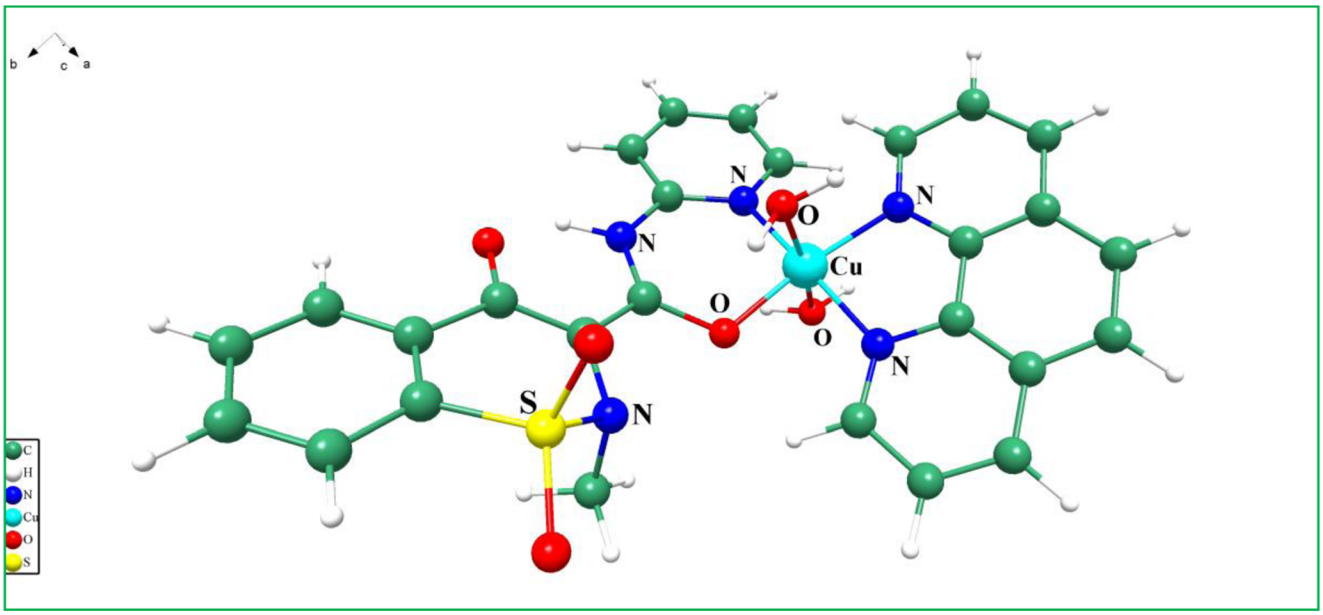

Fig. 2 The optimized structure of [Cu (Pir) (phen) $(H_2O)_2$] NO_3

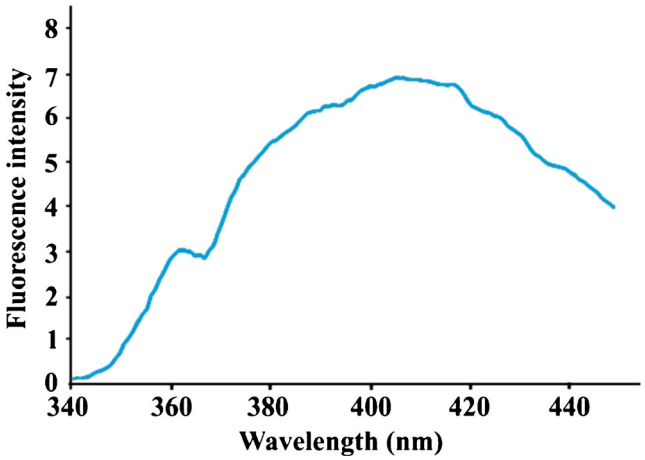

Fig. 3 Solid-state emission spectrum of the MC-C hybrid containing [Cu (Pir) (phen) $(H_2O)_2]^+$

FE-SEM Studies

The morphological images of Cloisite Na^+ and MCs-C were studied by FE-SEM. The FE-SEM images of Cloisite Na^+ show massive aggregated morphology and in some instances, there are some bulky flakes (Fig. 7a and b). After modification of Cloisite Na^+ with the cationic Ru (II) or Cu (II) complex, the morphology of the hybrid materials was changed. According to the FE-SEM results, the morphology of MCs-C has more fragments of smaller size, and they are formed with irregular shapes. The particle size of the MCs-C is between 15 and 30 nm (Fig. 7c-f).

Thermal Properties

A useful method for the characterization of the modified clays is thermal analysis technique [21, 30]. This method can be determined the thermal stability and thermal decomposition mechanism of the modified clays. The TGA analysis of MCs-C shows weight loss as a function of temperature in the range of 25 to 800 °C. The TGA curves for Cloisite Na^+ and MCs-C

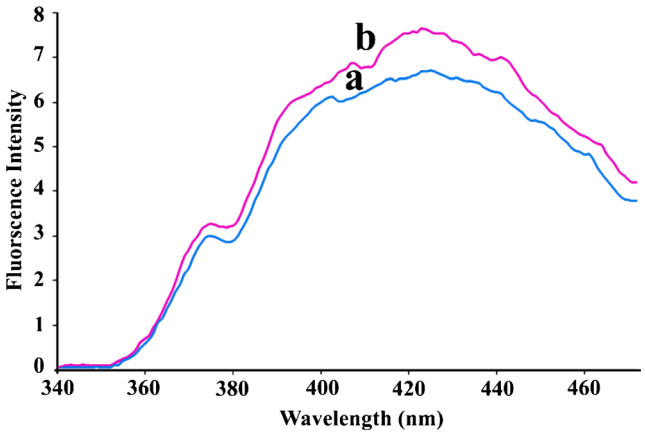

Fig. 4 Solid-state emission spectra of the pure [Ru (tpy)$_2$] $(PF_6)_2$ complex (**a**) and MC-C containing [Ru (tpy)$_2$]$^{2+}$ (**b**)

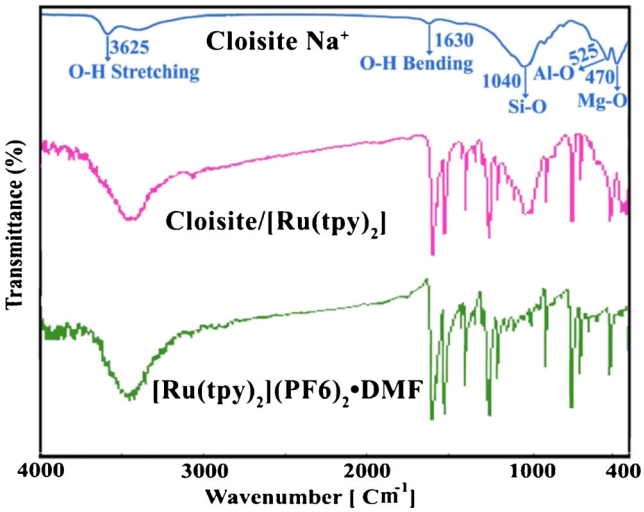

Fig. 5 FT-IR spectra of Cloisite Na^+, MC-C (M = Ru (II)) and [Ru (tpy)$_2$] $(PF_6)_2$

are illustrated in Fig. 8. The decomposition of Cloisite Na^+ occurs in two steps [21, 27]: one around 100 °C, which can be attributed to the desorption of water from the interlayer space, and the other is around 660 °C, which is due to dehydroxylation of the layers. The presence of a metal complex in the MCs-C increases the number of decomposition steps. In addition, the weight loss of interlayer water in the case of MCs-C is greater than the Cloisite Na^+. Due the intercalation of [Cu (Pir) (phen) $(H_2O)_2]^+$ or [Ru (tpy)$_2$]$^{2+}$ into the interlayer space of Cloisite, a larger free space is created, so the amount of water that can be absorbed is increased. In MCs-C, the number of decomposition steps was increased to four steps. The first step occurs around 90–110 °C due to the loss of water trapped

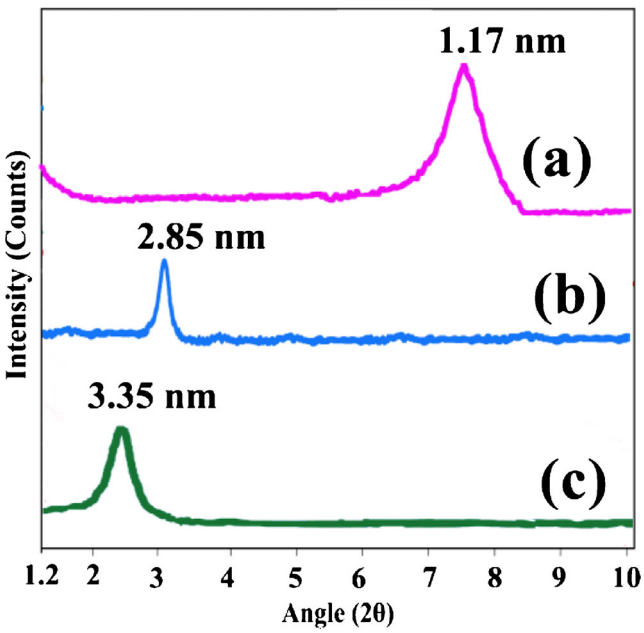

Fig. 6 XRD patterns of Cloisite Na^+ (**a**), MC-C (M = Cu (II)) (**b**) and MC-C (M = Ru (II)) (**c**)

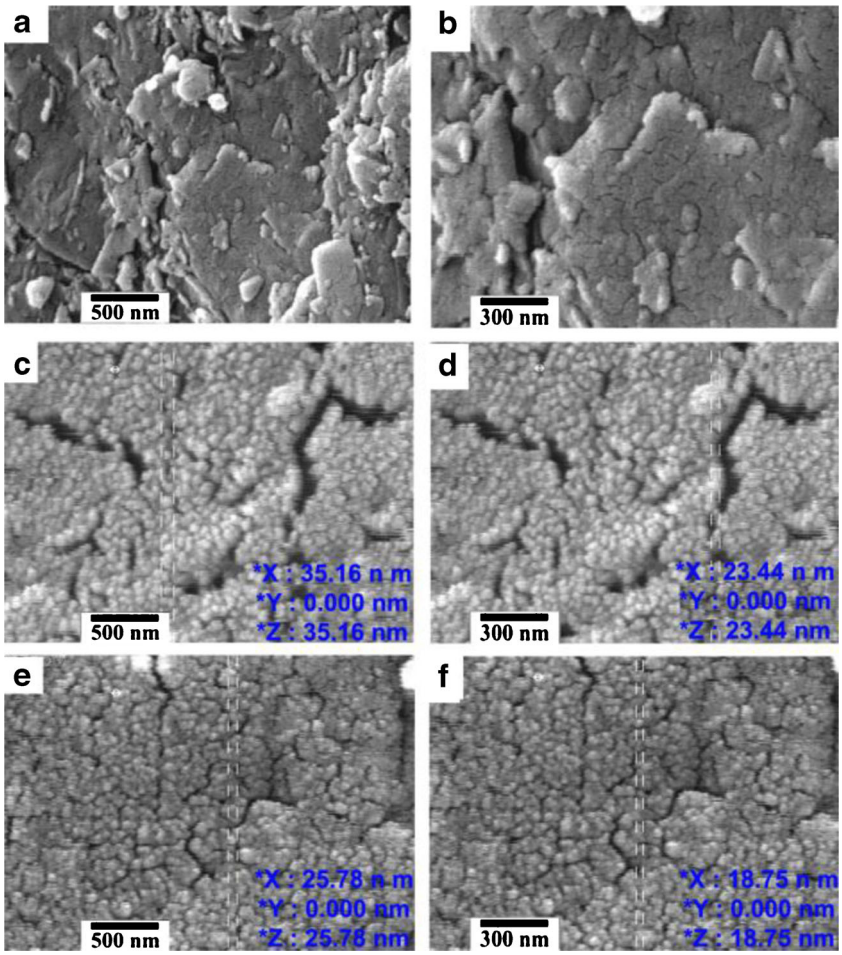

Fig. 7 FE-SEM images of Cloisite Na^+ (**a**, **b**), MC-C (*M* = Ru (II)) (**c**, **d**) and MC-C (*M* = Cu (II)) (**e**, **f**)

in MCs-C. The onset for decomposition of organic substance occurs around 200–300 °C with the maximum decomposition temperature around 260–275 °C. The third decomposition occurs at 450–500 °C, and finally the forth decomposition starts at around 560–620 °C due to the dehydroxylation of the structural OH units of Cloisite. According to Fig. 8, Cloisite Na^+ does not undergo thermally induced changes in the temperature range of 120–620 °C, therefore the mass loss in this temperature range should be attributed to the decomposition of the intercalated cationic complexes [21]. At 800 °C, the residue for MCs-C is up to 81 %. Also, the results show that the MC-C (M = Ru (II)) hybrid is more stable than the MC-C (M = Cu (II)) hybrid. As shown by XRD patterns and TGA curves, the cationic complexes have been successfully intercalated into the Cloisite layers.

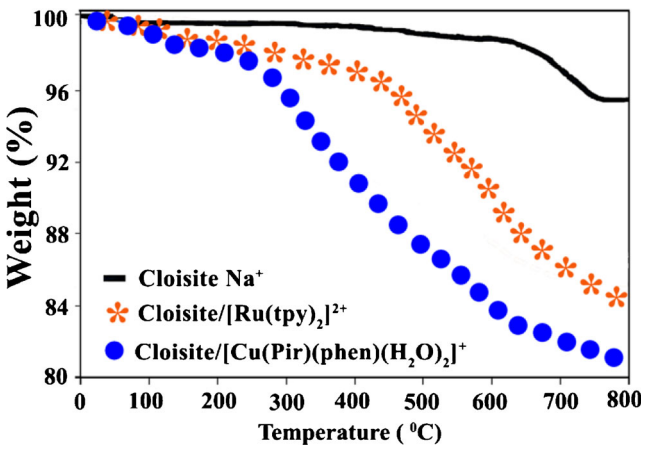

Fig. 8 TGA *curves* of Cloisite Na^+ and MCs-C

Conclusions

Two novel nanohybrid materials of Cloisite Na^+ with $[Ru(tpy)_2]^{2+}$ and $[Cu(Pir)(phen)(H_2O)_2]^+$, were synthesized by a simple and convenient way in an aqueous solution for the first time. FT-IR spectroscopy and XRD results show that the cationic complexes were intercalated into the Cloisite layers. The interlayer spaces of MCs-C are increased, which facilitates the intercalation of the host molecules into the interlayer space for further applications. The solid-state fluorescence properties of MCs-C show that both cationic complexes exhibit a significant fluorescence emission at room temperature when intercalated into Cloisite. The FE-SEM photographs of

MCs-C show a homogeneous morphology and the particle size is between 15 and 30 nm. The TGA results show that the modified clays verify stepwise decomposition corresponding to initial weight loss from the residual water desorption, followed by decomposition of the metal complex and the dehydroxylation of structural water of the clay layers.

Supplementary Material

CCDC 959787 contains the supplementary crystallographic data for [Ru (tpy)$_2$] (PF_6)$_2$·DMF. These data can be obtained free of charge via http://www.ccdc.cam.ac.uk/conts/retrieving.html, or from the Cambridge Crystallographic Data Centre, 12 Union Road, Cambridge CB2 1EZ, UK; fax: (+44) 1223-336-033; or e-mail: deposit@ccdc.cam.ac.uk.

Acknowledgments We wish to express our gratitude to the Research Affairs Division of Isfahan University of Technology (IUT) for partial financial support. Further financial support from the National Elite Foundation (NEF), Iran Nanotechnology Initiative Council (INIC) and the Center of Excellency in Sensors and Green Chemistry Research (IUT) is gratefully acknowledged.

References

1. Morimoto K, Nakae T, Ohara K, Tamura K, Nagaoka SI, Sato H (2012) Dual emitting Langmuir–Blodgett films of cationic iridium complexes and montmorillonite clay for oxygen sensing. New J Chem 36:2467–2471
2. Bezaatpour A, Behzad M, Jahed V, Amiri M, Mansoori Y, Rajabalizadeh Z, Sarvi S (2012) Cu (II) schiff base complexes on montmorillonite as nano-reactor heterogeneous catalysts for the epoxidation of cyclooctene: synthesis, characterization and immobilization. React Kinet Mech Cat 107:367–381
3. Ennajih H, Gueddar H, El Kadib A, Bouhfid R, Bousmina M, Essassi EM (2012) Intercalation of nickel and cobalt thiabendazole complexes into montmorillonite. Appl Clay Sci 65–66:139–142
4. Bagchi B, Kar S, Dey SK, Bhandary S, Roy D, Mukhopadhyay TK, Das S, Nandy P (2013) In situ synthesis and antibacterial activity of copper nanoparticle loaded natural montmorillonite clay based on contact inhibition and ion release. Colloids Surf B 108:358–365
5. Ayodele OB, Hameed BH (2013) Synthesis of copper pillared bentonite ferrioxalate catalyst for degradation of 4-nitrophenol in visible light assisted Fenton process. J Ind Eng Chem 19:966–974
6. Li Z, Ding H, Wu S, Liu H, Su H, Sun J, Zheng D, Huo Q, Guan J, Kan Q (2013) Tetraazamacrocycle complexes of Cu (II) and VO (IV) exchanged in the interlayers of montmorillonite clay: heterogeneous catalysts for the aerobic oxidation of styrene. Mater Res Bull 48: 1920–1926
7. Boukhatem H, Djouadi L, Abdelaziz N, Khalaf H (2013) Synthesis, characterization and photocatalytic activity of CdS-montmorillonite nanocomposites. Appl Clay Sci 72:44–48
8. Cao Z, Liao Z, Wang X, Su S, Feng J, Zhu J (2013) Preparation and properties of NBR composites filled with a novel black liquor-montmorillonite complex. J Appl Polym Sci 127:3725–3730
9. Wu Y, Zhou N, Li W, Gu H, Fan Y, Yuan J (2013) Long-term and controlled release of chlorhexidine-copper (II) from organically modified montmorillonite (OMMT) nanocomposites. Mater Sci Eng C 33:752–757
10. Kuźniarska-Biernacka I, Pereira C, Carvalho AP, Pires J, Freire C (2011) Epoxidation of olefins catalyzed by manganese (III) salen complexes grafted to porous heterostructured clays. Appl Clay Sci 53:195–203
11. Wang X, Wang D, Liang P, Liang X (2013) Synthesis and properties of an insoluble chitosan resin modified by azamacrocycle copper (II) complex for protein hydrolysis. J Appl Polym Sci 128:3280–3288
12. Kurokawa H, Nakazato Y, Tahara S, Katakura T, Ishihama Y, Sakuragi T, Miura H (2013) Copolymerization of ethylene with vinyl monomers using heterogeneous catalysts consisting of α-diimine Ni (II) complexes immobilized into a fluorotetrasilicic mica interlayer in the presence of an alkylaluminum compound. Macromol React Eng 7:125–134
13. Abbenhuis HCL (2000) Advances in homogeneous and heterogeneous catalysis with metal-containing silsesquioxanes. Chem Eur J 6: 25–32
14. Ruiz-Hitzky E, Van Meerbeeck A (2006) *Handbook of clay science*. F. Theng, B.K.G. Lagaly, (Eds.) Bergaya, Elsevier, Amsterdam
15. Takahashi T, Yamaguchi M (1991) Host-guest interaction between swelling clay minerals and poorly water-soluble drugs. 1: complex formation between a swelling clay mineral and griseofulvin. J Incl Phenom Macrocycl Chem 10:283–297
16. He H, Ma Y, Zhu J, Yuan P, Qing Y (2010) Organoclays prepared from montmorillonites with different cation exchange capacity and surfactant configureuration. Appl Clay Sci 48:67–72
17. Ke YC (2005) Stroeve P Polymer-layered silicate and silica nanocomposites. Amsterdam, the Netherlands.
18. Lagaly G, Ogawa M, Dekany I (2006) Clay mineral organic interactions. Handbook of Clay Science. F. Bergaya, B.K.G. Theng, G. Lagaly, (Eds) Chapter 7.3
19. Wang HW, Dong RX, Liu CL, Chang HY (2007) Effect of clay on properties of polyimide-clay nanocomposites. J Appl Polym Sci 104: 318–324
20. Adams JM, Gabbutt AJ (1990) Interaction of smectites with organic photochromic compounds. J Incl Phenom Macrocycl Chem 9:63–83
21. Mallakpour S, Dinari M (2013) Preparation, characterization, and thermal properties of organoclay hybrids based on trifunctional natural amino acids. J Therm Anal Calorim 111:611–618
22. Kakiage M, Ando S (2011) Effects of dispersion and arrangement of clay on thermal diffusivity of polyimide-clay nanocomposite film. J Appl Polym Sci 119:3010–3018
23. Isci S, Uslu YO, Ice OI (2009) The characterizations of rheological, electrokinetical and structural properties of ODTABr/MMT and HDTABr/MMT organoclays. Mater Charact 60:432–436
24. Dias PM, De Faria DLA, Constantino VRL (2000) Spectroscopic studies on the interaction of tetramethylpyridylporphyrins and cationic clays. J Incl Phenom Macrocycl Chem 38:251–266
25. Ma X, Lee NH, Oh HJ, Hwang JS, Kim SJ (2010) Preparation and characterization of silica/polyamide-imide nanocomposite thin films. Nanoscale Res Lett 5:1846–1851
26. Li F, Rosen MJ (2000) Adsorption of gemini and conventional cationic surfactants onto montmorillonite and the removal of some pollutants by the clay. J Colloid Interface Sci 224:265–271
27. Mallakpour S, Dinari M (2011) Preparation and characterization of new organoclays using natural amino acids and Cloisite Na^+. Appl Clay Sci 51:353–359
28. Mallakpour S, Dinari M, Hadadzadeh H (2013) Insertion of fluorophore dyes between Cloisite Na^+ layered for preparation of novel organoclays. J Incl Phenom Macrocycl Chem 77:463–470
29. Mallakpour S, Dinari M (2012) Synthesis and properties of biodegradable poly (vinyl alcohol)/ organo-nanoclay bionanocomposites. J Polym Environ 20:732–740
30. Zhao F, Wana C, Baoa X, Kandasubramanian B (2009) Modification of montmorillonite with aminopropylisooctyl polyhedral oligomeric silsequioxane. J Colloid Interface Sci 333:164–170